nature genetics

Deficiency of UBR1, a ubiquitin ligase of the N-end rule pathway, causes pancreatic dysfunction, malformations and mental retardation (Johanson-Blizzard syndrome)

Martin Zenker[1,20], Julia Mayerle[2,20], Markus M Lerch[2], Andreas Tagariello[1], Klaus Zerres[3], Peter R Durie[4], Matthias Beier[2], Georg Hülskamp[5], Celina Guzman[6], Helga Rehder[7], Frits A Beemer[8], Ben Hamel[9], Philippe Vanlieferinghen[10], Ruth Gershoni-Baruch[11], Marta W Vieira[12], Miroslav Dumic[13], Ron Auslender[14], Vera L Gil-da-Silva-Lopes[15], Simone Steinlicht[1], Manfred Rauh[16], Stavit A Shalev[17], Christian Thiel[1], Andreas Winterpacht[1], Yong Tae Kwon[18], Alexander Varshavsky[19] & André Reis[1]

Johanson-Blizzard syndrome (OMIM 243800) is an autosomal recessive disorder that includes congenital exocrine pancreatic insufficiency, multiple malformations such as nasal wing aplasia, and frequent mental retardation[1]. We mapped the disease-associated locus to chromosome 15q14–21.1 and identified mutations, mostly truncating ones, in the gene *UBR1* in 12 unrelated families with Johanson-Blizzard syndrome. *UBR1* encodes one of at least four functionally overlapping E3 ubiquitin ligases of the N-end rule pathway, a conserved proteolytic system whose substrates include proteins with destabilizing N-terminal residues[2–5]. Pancreas of individuals with Johanson-Blizzard syndrome did not express UBR1 and had intrauterine-onset destructive pancreatitis. In addition, we found that *Ubr1*$^{-/-}$ mice, whose previously reported phenotypes include reduced weight and behavioral abnormalities[6,7], had an exocrine pancreatic insufficiency, with impaired stimulus-secretion coupling and increased susceptibility to pancreatic injury. Our findings indicate that deficiency of UBR1 perturbs the pancreas' acinar cells and other organs, presumably owing to metabolic stabilization of specific substrates of the N-end rule pathway.

Since its initial description in 1971 (ref. 1), more than 60 cases of Johanson-Blizzard syndrome (JBS) have been reported. In addition to its pathognomonic features of congenital exocrine pancreatic insufficiency and nasal wing aplasia (**Fig. 1a**), JBS includes several facultative abnormalities, including scalp defects, imperforate anus, deafness, hypothyroidism, dental defects, genitourinary malformations and mental retardation[1,8–15]. Identification of seven cases of JBS in a European population-based study on imperforate anus[16], which occurs in 40% of individuals with JBS, suggests that the incidence of JBS is ~1 in 250,000.

To identify the locus mutated in JBS, we undertook a genome-wide linkage scan using a panel of microsatellite markers with average distance of 10 cM in seven kindreds with JBS (**Supplementary Fig. 1** online). We identified a region of homozygosity on chromosome 15q shared by individuals originating from all consanguineous families. We further analyzed this region by typing additional microsatellite markers from the draft human genome sequence and refined the candidate region to a 7.5-cM interval between the flanking markers *D15S1012* and *D15S659*. The maximum two-point lod score was 4.8 for $\theta = 0$ at *D15S968* (**Supplementary Table 1** online). We prioritized genes for mutational screening on the basis of putative function and expression data but identified no obvious candidate. By high-throughput direct sequencing of DNA from individuals with JBS, we eventually detected mutations in the gene *UBR1*. *UBR1* spans ~161 kb, contains 47 exons and encodes one E3 ubiquitin (Ub) ligase of the N-end rule pathway (**Fig. 1b,c**). In affected individuals from 12 of 13 families included in our study, the variations likely to be causal mutations were identified on both alleles of *UBR1*, whereas in one

[1]Institute of Human Genetics, University of Erlangen-Nuremberg, Schwabachanlage 10, 91054 Erlangen, Germany. [2]Department of Gastroenterology, Endocrinology and Nutrition, Ernst-Moritz-Arndt-University of Greifswald, Germany. [3]Institute of Human Genetics, University of Aachen, Germany. [4]Programme in Integrative Biology, the Research Institute, the Hospital for Sick Children, Toronto, Canada. [5]Department of Pediatrics, University of Muenster, Germany. [6]National Children's Hospital, University of Costa Rica, Costa Rica. [7]Department of Human Genetics, KIMCL, Medical University Vienna, Austria. [8]Department of Medical Genetics, University Utrecht, The Netherlands. [9]Department of Human Genetics, Radboud University Nijmegen Medical Centre, The Netherlands. [10]Department of Pediatrics, Unit of Neonatology, Hotel-Dieu, CHU, Clermont-Ferrand, France. [11]Department of Genetics, Rambam Medical Center, Haifa, Israel. [12]Department of Medical Genetics, Catholic University of São Paolo, Brazil. [13]Children's Hospital Rebro, University of Zagreb, Croatia. [14]Department of Obstetrics and Gynecology, Carmel Medical Center, Haifa, Israel. [15]Department of Medical Genetics, State University of Campinas, São Paulo, Brazil. [16]University Children's Hospital, Erlangen, Germany. [17]Genetic Institute, Ha'Emek Medical Center, Afula, Israel. [18]Center for Pharmacogenetics, School of Pharmacy, University of Pittsburgh, Pennsylvania, USA. [19]Division of Biology, California Institute of Technology, Pasadena, California, USA. [20]These authors contributed equally to this work. Correspondence should be addressed to M.Z. (mzenker@humgenet.uni-erlangen.de).

Received 28 July; accepted 8 September; published online 20 November 2005; doi:10.1038/ng1681

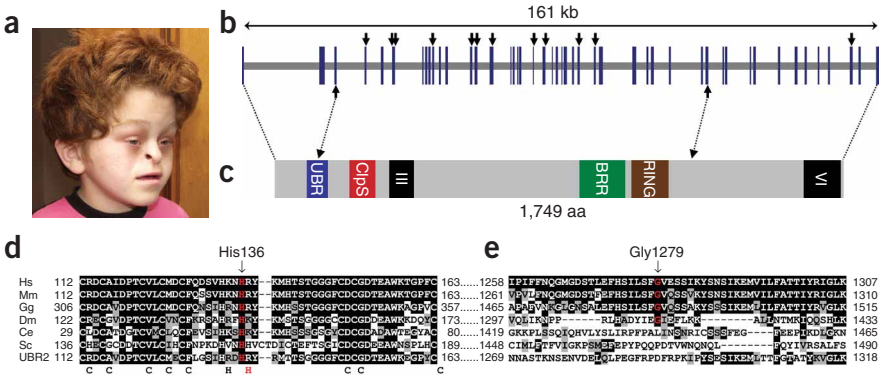

Figure 1 Clinical phenotype and *UBR1* mutations in JBS. (**a**) Typical clinical appearance of JBS with aplasia of the nasal wings in an 8-y-old female. (**b**) Exon-intron structure of *UBR1*, containing 47 exons (blue vertical bars). Sites of the mutations observed in JBS are indicated by arrows above for truncating mutations and below for two missense mutations (**c**). The UBR1 protein contains several distinct regions, including the UBR box (a substrate-binding domain), which is highly conserved among UBR family members[3], and the cysteine- and histidine-rich RING (RING-H2) domain, which is present in a larger class of E3 Ub ligases[6,7,28]. Regions III and IV denote sequences that are highly conserved among UBR1 and UBR2 in different species. ClpS denotes a region of sequence similarity to prokaryotic ClpS, an accessory subunit that contributes to recognition of degrons by the ATP-dependent protease ClpAP[29]. BRR (basic residue–rich region) denotes a conserved motif that contributes to the binding of yeast UBR1 to the E2 enzyme RAD6 (refs. 28,30). (**d**,**e**) Sequence alignments of two regions of human UBR1 with its orthologs in different species and with human UBR2. (**d**) The highly conserved residue His136 mutated in one case of JBS is located in the conserved zinc finger–like motif [C-X_{12}-]C-X_2-C-X_5-C-X_2-C-X_2-C-X_5-H-X_2-H-$X_{12\text{-}14}$-C-X_{11}-C, called the UBR box. (**e**) Gly1279, a residue of UBR1 mutated in another case of JBS, is located in a region of unknown function. The sequence context of Gly1279 in human UBR1 is less conserved than that of His136; the former context is different in putative *Drosophila melanogaster* UBR1 and in human UBR2. Black and gray shading indicates identical and similar residues, respectively. Hs, *Homo sapiens*; Mm, *Mus musculus*; Gg, *Gallus gallus*; Dm, *Drosophila melanogaster*; Ce, *Caenorhabditis elegans*; Sc, *Saccharomyces cerevisiae*.

family, only the paternally inherited mutation was found (**Table 1**). Most disease-associated *UBR1* alleles (12 of 14) were mutations that predicted premature translational stop codons. Two missense mutations in *UBR1* caused substitutions of residues that are conserved among UBR1 proteins of different species (**Fig. 1d**,**e**). One of these missense mutations, H136D, affected a conserved motif in the region of UBR1 previously found to be important for substrate binding[3] and was therefore likely to perturb the activity of UBR1. Two apparently unrelated and nonconsanguineous families originating from the same district in Costa Rica shared the same homozygous mutation Q513X. Haplotype analysis in these families provided evidence of a common ancestor (data not shown). In each family, the *UBR1* mutations segregated with the disease phenotype. None of the mutations was detected among 192 control chromosomes.

Using antibody to UBR1 and either immunofluorescence microscopy with pancreatic tissue sections or immunoblotting with extracts from cells in culture, we observed no UBR1 protein in individuals with JBS from different families, confirming that loss of UBR1 function is the mechanism underlying this disease (**Fig. 2a**,**d**). By contrast, UBR1 was readily detectable in control pancreas, where it was present largely in the cytosol of acinar cells (**Fig. 2b**). Control immunostaining for trypsinogen as a specific marker for acinar cells showed no substantial differences between pancreas from controls and individuals with JBS (**Fig. 2c**,**e**), indicating that there was no primary defect of zymogen synthesis in JBS.

The N-end rule pathway is a part of the Ub-proteasome system[2–7,17]. Regulated protein degradation by this system controls the levels of many intracellular proteins[18,19]. A substrate of the Ub system is conjugated to Ub through the action of three enzymes, E1, E2 and E3; the latter group is an exceptionally large set of proteins[18,19]. A ubiquitylated protein bears a covalently linked poly-Ub chain and is degraded by the 26S proteasome[18]. The selectivity of ubiquitylation is determined mainly by E3, which recognizes a substrate's degradation signal (degron)[4,18]. We found that UBR1 is another of the E3 Ub ligases that are implicated in the pathogenesis of human genetic diseases. These E3 ligases include UBE3A, mutant in Angelman

Table 1 ***UBR1*** **mutations detected in 13 families with JBS**

Family	Ethnic origin	Parental consanguinity	Nucleotide alteration	Alteration in coding sequence	Exon	Status[a]	Ref.
JBS01	Turkish	Yes	1648C→T	Q550X	14	Hom	–
JBS02	Turkish	Yes	1759C→T	Q587X	15	Hom	–
JBS03	Costa Rican Indian	No	1537C→T	Q513X	13	Hom	9
JBS04	Costa Rican Indian	No	1537C→T	Q513X	13	Hom	–
JBS05	Dutch	No	407A→G; IVS20+2T→C	H136R; abnormal splicing	3; 20[b]	Het; Het	–
JBS06	Turkish	Yes	IVS21+1G→C	Abnormal splicing	21[b]	Hom	11
JBS07	German	No	IVS5-2delAG; 3835G→A	Abnormal splicing; G1279S	6[c]; 35	Het; Het	15
JBS08	Dutch	No	2547insA	M849fsX861	27	Het[d]	12
JBS09	Turkish	Yes	4927G→T	E1643X	45	Hom	13
JBS10	Portuguese	Yes	477delT	T159fsX164	4	Hom	21
JBS11	Indian	Yes	753-754delTG	C251X	6	Hom	21
JBS12	African	Yes	IVS9-12A→G	Abnormal splicing	10[e]	Hom	14
JBS13	Israeli Arab	Yes	2598delA	P866fsX878	28	Hom	–

[a]Het, heterozygous; Hom, homozygous. [b]Mutation deletes the consensus splice donor. [c]Mutation deletes the consensus splice acceptor. [d]The second mutation was not detected in this individual, suggesting that it is located in intronic or promoter regions, which were not sequenced. [e]Mutation creates an ectopic splice acceptor predicted to replace the authentic splice site.

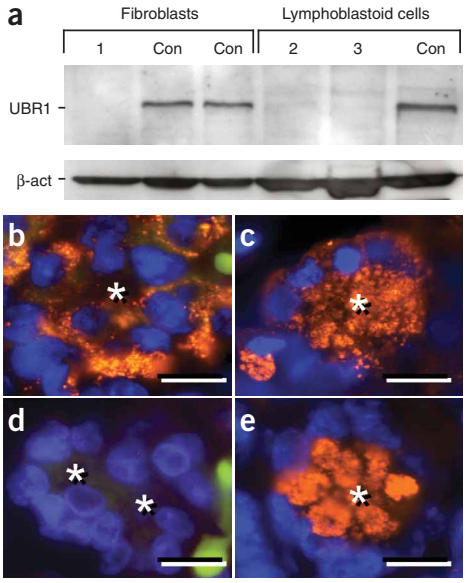

Figure 2 The absence of UBR1 protein in individuals with JBS. (**a**) UBR1-specific immunoblotting of extracts from fibroblast and lymphoblastoid cells derived from three different individuals with JBS (1 from family JBS01; 2 from family JBS02; and 3 from family JBS08). Note the absence of the band of 200-kDa UBR1 in JBS samples versus controls (Con). Immunoblotting for β-actin (β-act) served as a loading control. (**b**–**e**) Immunofluorescence patterns in sections of a normal pancreas (**b**,**c**) versus that of a newborn individual with JBS (from family JBS02; **d**,**e**). Tissue sections were immunostained for UBR1 (**b**,**d**) and trypsinogen (**c**,**e**), the latter as a marker for acinar cells. Normal pancreas shows intense UBR1-specific (**b**) and trypsinogen-specific (**c**) staining in the secretory compartment of acinar cells. In contrast, the UBR1-specific staining is absent in pancreatic acini from the individual with JBS (**d**), whereas trypsinogen-specific staining is intact in residual acini from the individual with JBS (**e**). DAPI was used for nuclear counterstaining. Asterisks indicate centers of individual acini. Scale bars, 200 μm.

syndrome (OMIM 105830); parkin, mutant in autosomal-recessive juvenile parkinsonism (OMIM 600116); and VHL, mutant in von Hippel-Lindau disease (OMIM 193300)[18–20].

The N-end rule relates the *in vivo* half-life of a protein to the identity of its N-terminal residue[3,4,7,17]. It has a hierarchic structure: some destabilizing N-terminal residues are enzymatically modified before they are recognized by the pathway's Ub ligases, including UBR1. Known functions of the N-end rule pathway include control of peptide import (through conditional degradation of import's repressor), regulation of apoptosis (through degradation of a caspase-processed inhibitor of apoptosis), fidelity of chromosome segregation (through degradation of a conditionally produced fragment of cohesin), regulation of meiosis and cardiovascular development[2,3,6,7,17].

Mammalian UBR1 contains distinct binding sites for basic (type 1) and bulky hydrophobic (type 2) N-terminal residues of substrates, as well as a third binding site for substrates bearing internal (non-N-terminal) degrons[3,4,6,7,17]. The family of mouse (and human) UBR proteins, which contain a common substrate-binding domain called the UBR box, consists of at least four E3 ligases, including UBR1 and UBR2 (ref. 3). The latter have similar substrate-binding properties[6,7]. Functional overlaps among these E3 ligases probably underlie the viability of single-mutant mice[6,7] (*Ubr1*$^{-/-}$ and *Ubr2*$^{-/-}$) and the more severe but still nonlethal phenotype of individuals with JBS. Double mutant *Ubr1*$^{-/-}$*Ubr2*$^{-/-}$ mice undergo early embryonic lethality[3,6].

We examined the possibility that aspects of the JBS phenotype might stem from reduced expression of (possibly) UBR1-complementing UBR2 E3 ligase in organs most prominently affected in JBS. But the two genes were expressed at similar levels in all tissues that we examined, including adult and fetal pancreas (**Supplementary Fig. 2** online). These results suggested that the phenotypes of JBS may be caused by molecular perturbations that were specific to the absence of UBR1, as they could not be rescued by UBR2.

To address further the pathogenesis of JBS, we focused on exocrine pancreas, an organ most consistently affected in this disease[21]. Autopsy findings previously suggested that exocrine pancreatic insufficiency in individuals with JBS was caused by selective loss of acinar cells[8,10,13], but details of this process remained to be elucidated. We examined pancreatic pathology and cell biology in autopsy specimens from two fetuses (21 and 34 weeks of gestation, respectively) and also in a newborn baby with JBS. The pancreas of individuals with JBS showed acinar tissue loss that increased with gestational age and was accompanied by inflammatory infiltrates, most prominent in the near-term fetus (**Fig. 3**). Using the TUNEL assay for apoptotic cells, we found no evidence of increased apoptosis in acinar cells of individuals with JBS (data not shown). Taken together, these findings suggest that the main pancreatic defect in individuals with JBS is not perturbed acinar development in early embryogenesis, but rather gradual destruction of previously formed acinar cells in maturing fetuses, a process that resembles pancreatitis of intrauterine onset.

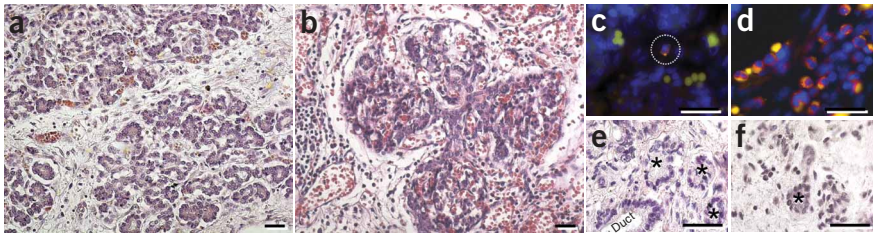

Figure 3 Characterization of human pancreas in JBS. Paraffin sections of the pancreas of a prematurely born (34 weeks of gestation) proband from family JBS02 (**b**,**d**) were compared with those of a control of the same gestational age (**a**,**c**). Hematoxylin and eosin staining in the individual with JBS (**b**) shows large areas of loss of the acinar tissue, hypervascularization, depositions of connective tissue and prominent inflammatory infiltrates. Remaining pancreatic acini have an apparently normal architecture. An age-matched control is shown in **a**. Scale bars, 250 μm. (**c**,**d**) Immunostaining for CD45, a common leukocyte marker, in the same individual with JBS (**d**) and the control (**c**) confirms that the pancreatic infiltrates consist mainly of CD45-positive cells (red fluorescence), but no such cells are seen in the control pancreas (**c**), with one exception, denoted by a circle. Areas of green staining are caused by autofluorescence of erythrocytes. DAPI was used to counterstain the nuclei. (**e**) A representative section of pancreatic tissue from a fetus with JBS at 21 weeks of gestation (from family JBS09) shows normal developing acini (asterisks) and relatively few leukocytes. (**f**) In contrast, the pancreas of a term newborn from the same family has few areas of remaining acini (asterisk), and the parenchyma is largely replaced by connective tissue.

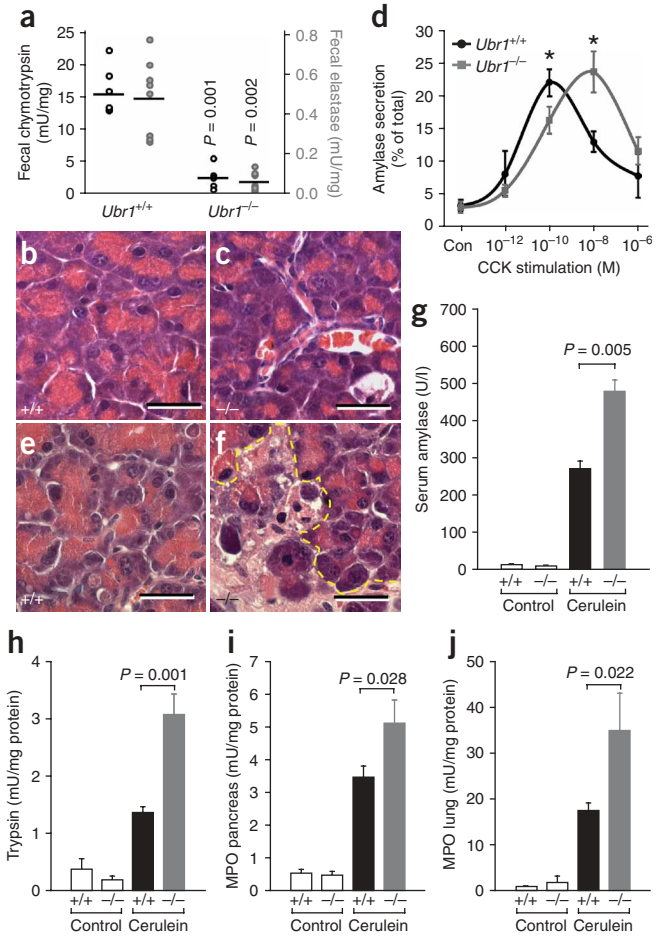

Figure 4 Characterization of pancreatic abnormalities in *Ubr1*$^{-/-}$ mice. (**a**) Chymotrypsin and elastase measurements in mouse feces indicate that activities were substantially lower in *Ubr1*$^{-/-}$ mice ($n = 8$) than in controls ($n = 8$). (**b**,**c**) With hematoxylin and eosin staining, the pancreas of adult *Ubr1*$^{-/-}$ mice (**c**) showed no obvious morphological abnormalities versus controls (**b**). Scale bars, 300 μm. (**d**) Amylase release was determined in freshly isolated pancreatic acini incubated with increasing concentrations of the secretagogue cholecystokinin (CCK; 10^{-12} M to 10^{-6} M). Wild-type acini showed maximal secretion at 10^{-10} M cholecystokinin, whereas the maximum shifted up by a factor of ~100 (to 10^{-8} M cholecystokinin) with *Ubr1*$^{-/-}$ acini, indicative of an impaired stimulus-secretion coupling in *Ubr1*$^{-/-}$ pancreas. $^*P < 0.005$. (**e**,**f**) Hematoxylin and eosin–stained sections after *in vivo* induction of pancreatitis by supramaximal amounts of cerulein. This treatment is known to lead to a paradoxical block of pancreatic secretion and intracellular zymogen activation, eventually resulting in acinar cell necrosis and local as well as systemic inflammatory response[23]. Compared with wild-type mice (**e**), *Ubr1*$^{-/-}$ mice (**f**) had increased areas of necrotic cells (yellow dashed line). Consistent with these findings, serum amylase levels were significantly higher in *Ubr1*$^{-/-}$ mice (**g**). In pancreatic homogenates from *Ubr1*$^{-/-}$ mice treated with cerulein, we also found significantly higher trypsin activity, in comparison with identically treated wild-type mice, but there was no increased spontaneous trypsin activity in untreated *Ubr1*$^{-/-}$ mice versus wild-type mice (**h**). Quantification of MPO activity in pancreatic homogenates and the lungs, reflecting, respectively, local and systemic inflammatory responses to experimental pancreatitis, showed significantly increased MPO levels in *Ubr1*$^{-/-}$ mice (**i**,**j**). For each group ($n = 6$), error bars represent s.d.

To analyze molecular aspects of perturbations in JBS that would be difficult or impossible to address in human autopsy material, we used *Ubr1*$^{-/-}$ mice[3,6,7]. These mice were viable and fertile and lacked substantial phenotypic abnormalities other than reduced weight (by 10–20%, with disproportionate decreases in skeletal muscle and adipose tissue)[7]. To examine whether malnutrition due to exocrine pancreatic insufficiency could be one cause of reduced weight of *Ubr1*$^{-/-}$ mice, we determined fecal chymotrypsin and elastase activity and detected impaired pancreatic exocrine function (**Fig. 4a**). We excluded the possibilities that synthesis of trypsinogen and proelastase was markedly reduced and that defects in their activation caused the pancreatic impairment by measuring protein content and pancreatic tissue activities of these enzymes in *Ubr1*$^{-/-}$ and wild-type mice (data not shown). In addition, we observed no substantial morphological differences between the pancreas of *Ubr1*$^{-/-}$ versus wild-type mice under control conditions, by either light or electron microscopy (**Fig. 4b**,**c** and data not shown).

To address these issues further, we prepared pancreatic acini (the functional assemblies of exocrine cells) from *Ubr1*$^{-/-}$ and wild-type mice and exposed them *in vitro* to increasing concentrations of the physiological secretagogue cholecystokinin[22]. Pancreas of *Ubr1*$^{-/-}$ mice was considerably (~100 times) less responsive to stimulation (**Fig. 4d**). This difference probably accounts for the observed metabolic defect and pancreatic insufficiency in *Ubr1*$^{-/-}$ mice and suggests that a signaling circuit that couples the secretion of pancreatic enzymes to the level of a secretion-causing compound is controlled by the N-end rule pathway. Further analysis used an *in vivo* model of acinar cell stress and experimental pancreatitis in which supraphysiological concentrations of secretagogue result in a 'paradoxical' block of pancreatic secretion[23]. We found that this treatment led to a more severe injury of *Ubr1*$^{-/-}$ pancreas, compared with wild-type, with prominent necrosis in the former, as indicated by histological evidence, serum amylase levels and other parameters of local pancreatic injury or systemic inflammatory response[23] (**Fig. 4e–j**). These results strongly suggest that the intact (as distinguished from UBR1-deficient) N-end rule pathway contributes to pancreatic homeostasis and defense against noxious stimuli in pancreatic acinar cells.

Taken together, our findings in UBR1-deficient mice and humans are consistent with the hypothesis that specific targets of UBR1 in the pancreas may include zymogens or their derivatives and molecules involved in their intracellular processing or export. The observed difference in phenotypic severity of UBR1 deficiency between human JBS and its mouse *Ubr1*$^{-/-}$ counterpart[3,6,7] may stem from species-specific differences in functional overlaps among Ub ligases of the N-end rule pathway. The phenotypic defects in JBS involve, in a consistently recurring pattern, several organ systems in addition to pancreas[1,8–15]. We suggest that UBR1-mediated protein degradation has a crucial role at certain stages of human development, in specific cell types, and that in those settings, this role cannot be effectively taken on by other E3 ligases of the N-end rule pathway. Further advances in understanding JBS will require identification of specific UBR1 substrates whose levels or functions are perturbed in the absence of UBR1 in ways that underlie the pathogenesis of JBS.

METHODS

Subjects. This study was approved by the University of Erlangen-Nuremberg Institutional Review Boards. We obtained blood samples and pedigrees after receiving informed consent from the parents or caretakers of the individuals affected by JBS. We extracted genomic DNA using standard procedures. From deceased individuals and aborted fetuses, we obtained DNA from stored biopsy specimens, either cryoconserved or paraffin-embedded. Several of our subjects were previously reported (**Table 1**). Of the 15 families diagnosed with JBS that we studied, two were excluded from further study: in one case, only paraffin-embedded fixed tissue that did not yield DNA of acceptable quality

was available from the index individuals, and the other case, there were concerns about the clinical diagnosis of JBS in the index individual. All other subjects had the unequivocal clinical picture of JBS, with congenital exocrine pancreatic insufficiency and severe hypoplasia or aplasia of the nasal wings (these two traits are the minimal diagnostic criteria).

Linkage analysis. We carried out the initial genome-wide linkage analysis in families JBS01–JBS04, JBS06 and JBS09 using Weber panel Version 10 (Research Genetics), ABI3100 sequence analyzer and Genotyper software v3.7 (Applied Biosystems). We achieved marker saturation using existing and newly generated microsatellite markers. We carried out two-point lod score calculations using the LINKAGE program package, with help from the computer programs LINKRUN and MKS, using an autosomal recessive, fully penetrant model.

Mutation analysis. We identified candidate genes using the National Center for Biotechnology Information and University of California Santa Cruz human genome databases. We designed primers flanking each of the 47 exons of *UBR1*, as well as exons of other genes located in the critical interval, using standard software (Primer 3). Oligonucleotide sequences are given in **Supplementary Table 2** online. We carried out bidirectional direct sequencing using the BigDye Terminator Cycle Sequencing Kit (Applied Biosystems) and a ABI3730 capillary sequencer (Applied Biosystems). We evaluated the sequences using the DNA Star software.

Antibodies. We used a previously described[7] affinity-purified, peptide-mediated antibody to mouse UBR1, which is known to cross-react with human UBR1 (ref. 24). We used fluorescein isothiocyanate–conjugated mouse monoclonal antibody to human CD45 (Leukocyte Common Antigen) to label leukocytes in paraffin sections (BD Pharmingen, clone OX-1). We used a polyclonal antibody to human cationic trypsinogen from Chemicon International. We purchased mouse monoclonal antibody to human chymotrypsin from QED Bioscience.

Immunoblot analysis. We carried out immunoblot analyses with extracts from fibroblasts of individuals with JBS and JBS-derived lymphoblastoid cell lines versus wild-type controls. Equal amounts of total protein were separated by SDS-PAGE using NuPAGE 3–8% Tris Acetate Gel (Invitrogen), transferred to nitrocellulose membranes and probed with antibodies, using standard protocols and ECL-based detection with a Lumi-Imager F1 (Roche), in accordance with the manufacturer's instructions. We used immunoblotting with antibody to β-actin (Abcam) as a loading control.

Quantification of *UBR1* and *UBR2* expression using real-time RT-PCR. We isolated total RNA from human tissues using Trizol Reagent (Invitrogen) and synthesized cDNA using the SuperScript III One Step RT-PCR System (Invitrogen). We carried out real-time quantitative PCR in accordance with the manufacturer's instructions, using ABI PRISM 7900 (Applied Biosystems) and Assay-on-Demand TaqMan probe and primers (Hs00233297_m1 for *UBR1* and Hs00322358_m1 for *UBR2*). All reactions were run in triplicate. We calculated the levels of a target mRNA relative to two different reference mRNAs (*ACTB* and *B2M*). Assuming an efficiency of 2 (relative increase in template mRNA required to decrease by 1 the number of cycles), we calculated the relative expression ratios as $R = 2^{(Ct(control) - Ct(test))}$, where Ct is the cycle number at threshold.

Animals. For animal studies, we used a previously constructed strain of *Ubr1*$^{-/-}$ mice, in the C57BL6/129 mixed background[7]. Wild-type littermates served as controls. All animal studies were approved by the Animal Use and Care Committee of the University of Greifswald.

***In situ* RNA hybridization.** We cloned ~500-bp cDNA fragments into pCRII using the TA Cloning kit (Invitrogen). The resulting plasmid was digested with *Xba*I and then transcribed with SP6 RNA Polymerase (Roche). We selected the PCR-produced probes using the sequences of human *UBR1* (nucleotides (nt) 4,697–5,181) and *UBR2* (nt 4,712–5,198) and of mouse *Ubr1* (nt 4,984–5,486) and *Ubr2* (nt 4,839–5,270), choosing regions that yielded low scores in similarity comparisons among the UBR family members. We carried out *in situ* hybridization for mouse and human *UBR1* and *UBR2* with dissected pancreas of C57BL6 newborn mice and also with adult human pancreas obtained from a pancreatectomy specimen. We cut tissues into 10-μm-thick cryosections and examined them on Superfrost/Plus Microscope slides (Fisher Scientific). Additional probes derived from different parts of the human and mouse genes yielded similar results. Negative control probes yielded no specific hybridization in pancreas tissue (data not shown).

Induction of acute pancreatitis by cerulein. We induced pancreatitis in 6- to 8-week-old *Ubr1*$^{-/-}$ mice and wild-type littermates weighing 20–24 g. After fasting mice for 18 h, with access to water *ad libitum*, we administered the secretagogue cerulein (Pharmacia Biotech AB) using seven intraperitoneal injections of 50 μg per kg of body weight at hourly intervals, as described previously[23]. As controls, we used mice injected with saline solution. After exsanguination under ether anesthesia, the pancreas was rapidly removed, the fat was trimmed off, and the pancreas was either fixed in 5% formaldehyde for electron microscopy or embedded in paraffin. The main part of pancreas was frozen in LN_2 and stored at –80 °C until further analyses. Lung tissue was either fixed in 5% formaldehyde for morphology studies or snap-frozen in LN_2.

Amylase secretion assay. We carried out amylase secretion experiments as described previously[25]. Pancreas from male *Ubr1*$^{-/-}$ or wild-type mice was digested with purified collagenase (Collagenase Serva), mechanically dispersed and passed through a mesh nylon cloth. We incubated acini for 30 min at 37 °C with cholecystokinin (biologically active phosphorylated CCK octapeptide ([Tyr(SO3H)27]-cholecystokinin fragment; Sigma) at concentrations of 1 pM to 10 μM. We used unstimulated acini as controls. We measured amylase content in cell pellets and supernatants after lysing cells with ice-cold lysis buffer, using an amylase-mediated color reaction and ET-G_7PNP as a substrate (Amyl Kit; Roche). Amylase activity was expressed as a percentage of total amylase activity in the cells. Each group of assays comprised four independent experiments, and measurements were made in triplicate.

Immunofluorescence analysis in paraffin sections. We removed the paraffin from sections (2- to 4-μm) of paraffin-embedded tissues using standard procedures and processed them for immunolabeling as described[26]. We carried out immunostaining for trypsin, chymotrypsin, UBR1 and CD45. We detected apoptosis using the ApopTag Fluorescein *in situ* detection kit (S7110, Chemicon) in accordance with the manufacturer's instructions. This assay detects apoptotic cells *in situ* by the indirect TUNEL method. We counterstained nuclei using DAPI. We also stained paraffin-embedded sections with hematoxylin and eosin. We used a Zeiss Axiophot microscope connected to MR color digital camera for morphometric evaluation.

Electron microscopy. We fixed small blocks (2 mm in diameter) of pancreatic tissue from individuals with JBS or from pancreatitic and control mice in 2% formaldehyde-2% glutaraldehyde for Epon embedding, followed by osmium, uranyl and lead staining for electron microscopy of thin sections. Samples were examined using a Philips 400 electron microscope, as described[26].

Myeloperoxidase activity in lung and pancreatic homogenates. We processed tissues as previously described[23]. We homogenized pancreas or lung tissue and resuspended the pellet in 50 mM K-phosphate buffer (pH 6.0) containing 0.5% cetyltrimethylammoniumbromide. We measured myeloperoxidase (MPO) activity using 0.53 mM O-dianisidine and 0.15 mM H_2O_2 as substrates. We monitored the increase in A_{460} at room temperature, using a Dynatech MR 5000 Elisa reader. The results are expressed as units of MPO activity, with 1 unit corresponding to oxidation of 1 μmol H_2O_2 per min per mg of pancreatic protein.

Amylase serum levels. We collected blood by aortic puncture during killing of mice. We produced serum using standard procedures and stored it at –20 °C. We measured the activity of serum α-amylase using 4.6-ethylidene-(G7)-1-4-nitrophenyl-(GI)-α, D-maltoheptaoside (EPS method) in accordance with the manufacturer's protocol (Roche).

Detection of chymotrypsin and elastase in mouse feces. We collected the feces of *Ubr1*$^{-/-}$ mice and their wild-type littermates (fed standard chow) and stored it at –20 °C. We suspended samples of 15–30 mg in sample solvent (0.1% Triton X-100, 0.5 M NaCl and 100 mM $CaCl_2$), briefly sonicated them and centrifuged them at 20,000 r.p.m. for 10 min at 0 °C. We subjected the supernatant to fluorometric analysis. We used 10 μM

R110-(CBZ-Ala$_4$)$_2$-substrate (Molecular Probes) and 5 μM AMC-(Suc-Ala$_2$-Pro-Phe) (Bachem) to measure the elastase and chymotrypsin activities, respectively. Initial rates of substrate hydrolysis were plotted in arbitrary fluorescence units per min. Enzymatic activities were calculated as U mg^{-1} with purified elastase or chymotrypsin as internal standard, and the activities were stated in relation to fecal weight.

Detection of protease activity in pancreatic homogenates. We determined protease activity in pancreatic tissue as previously described[27]. We homogenized tissue samples with a Dounce-S glass homogenizer (Braun-Melsungen) in ice-cold 0.1 M Tris-HCl (pH 8.0) containing 5 mM $CaCl_2$. We determined protein concentrations using a modified Bradford assay (BioRad). In the pancreatic homogenates from *Ubr1*$^{-/-}$ or wild-type controls, we measured spontaneous trypsin activity as well as enterokinase activated (0.001 U ml^{-1}, 60 min at 37°C) trypsin activity with unstimulated pancreas or after supramaximal cerulein stimulation over 8 h, using the specific fluorogenic substrate [CBZ-Ile-Pro-Arg]-R110. We also determined spontaneous elastase activity as well as enterokinase-activated elastase activity using [CBZ-Ala]$_4$-R110, a specific fluorogenic substrate. We plotted initial rates of substrate hydrolysis in arbitrary fluorescence units per min, as described[25]. Measured enzymatic activities were calibrated against the activity of bovine trypsinogen or bovine elastase activated with enterokinase (0.001 U ml^{-1}, 60 min at 37°C) as standards and expressed as U mg^{-1} protein[27].

Data presentation and statistical analysis. Data in graphs are expressed as mean ± s.d. Statistical comparison of groups was done using Mann-Whitney rank-sum test, followed by Student's *t*-test for independent samples using SigmaStat and SigmaPlot (SPSS Inc.), which were also used for data presentation. We used at least five mice in each experiment. Differences were considered significant at a level of $P < 0.05$.

URLs. The human genome databases are available at http://genome.ucsc.edu/ and http://www.ncbi.nlm.nih.gov/. Primer 3 is available at http://www.broad.mit.edu/cgi-bin/primer/primer3_www.cgi/. The Online Mendelian Inheritance in Man (OMIM) database is available at http://www.ncbi.nlm.nih.gov/entrez/query.fcgi?db=OMIM. *In situ* hybridization was done as described at http://genetics.med.harvard.edu/~cepko/protocol.

Accession codes. GenBank: human *UBR1* mRNA, NM_174916. GenBank Protein: human UBR1 protein, AAL32103; mouse UBR1 protein, AAC40165; chicken UBR1 protein, XP_421165; fruit fly CG9086-PA protein, AAF48687; *Caenorhabditis elegans* ubiquitin ligase E3, AAB42328; yeast UBR1, NP_011700; human UBR2, AAH64512.

Note: Supplementary information is available on the Nature Genetics website.

ACKNOWLEDGMENTS

We thank all participating families for making this study possible; A. Diem, E. Dazert and S. Balk for technical assistance; and G. Nürnberg for lod score calculations. This research was supported by grants from the Marohn Foundation of the University of Erlangen-Nuremberg and from the German Research Foundation to M.Z. and A.R., from the German Research Foundation and the Deutsche Krebshilfe to M.M.L. and J.M. and from the US National Institutes of Health and the Ellison Medical Foundation to A.V. and Y.T.K.

COMPETING INTERESTS STATEMENT

The authors declare that they have no competing financial interests.

Published online at http://www.nature.com/naturegenetics/
Reprints and permissions information is available online at http://npg.nature.com/reprintsandpermissions/

1. Johanson, A. & Blizzard, R. A syndrome of congenital aplasia of the alae nasi, deafness, hypothyroidism, dwarfism, absent permanent teeth, and malabsorption. *J. Pediatr.* **79**, 982–987 (1971).
2. Kwon, Y.T. *et al.* An essential role of N-terminal arginylation in cardiovascular development. *Science* **297**, 96–99 (2002).
3. Tasaki, T. *et al.* A family of mammalian E3 ubiquitin ligases that contain the UBR box motif and recognize N-degrons. *Mol. Cell. Biol.* **25**, 7120–7136 (2005).
4. Varshavsky, A. The N-end rule: functions, mysteries, uses. *Proc. Natl. Acad. Sci. USA* **93**, 12142–12149 (1996).
5. Bachmair, A., Finley, D. & Varshavsky, A. In vivo half-life of a protein is a function of its amino-terminal residue. *Science* **234**, 179–186 (1986).
6. Kwon, Y.T. *et al.* Female lethality and apoptosis of spermatocytes in mice lacking the UBR2 ubiquitin ligase of the N-end rule pathway. *Mol. Cell. Biol.* **23**, 8255–8271 (2003).
7. Kwon, Y.T., Xia, Z., Davydov, I.V., Lecker, S.H. & Varshavsky, A. Construction and analysis of mouse strains lacking the ubiquitin ligase UBR1 (E3alpha) of the N-end rule pathway. *Mol. Cell. Biol.* **21**, 8007–8021 (2001).
8. Daentl, D.L., Frias, J.L., Gilbert, E.F. & Opitz, J.M. The Johanson-Blizzard syndrome: case report and autopsy findings. *Am. J. Med. Genet.* **3**, 129–135 (1979).
9. Guzman, C. & Carranza, A. Two siblings with exocrine pancreatic hypoplasia and orofacial malformations (Donlan syndrome and Johanson-Blizzard syndrome). *J. Pediatr. Gastroenterol. Nutr.* **25**, 350–353 (1997).
10. Moeschler, J.B., Polak, M.J., Jenkins, J.J. III & Amato, R.S. The Johanson-Blizzard syndrome: a second report of full autopsy findings. *Am. J. Med. Genet.* **26**, 133–138 (1987).
11. Rudnik-Schoneborn, S. *et al.* [Johanson-Blizzard syndrome]. *Klin. Padiatr.* **203**, 33–38 (1991).
12. Swanenburg de Veye, H.F., Heineman-de-Boer, J.A. & Beemer, F.A. A child of high intelligence with the Johanson-Blizzard syndrome. *Genet. Couns.* **2**, 21–25 (1991).
13. Vanlieferinghen, P.H., Borderon, C., Francannet, C.H., Gembara, P. & Dechelotte, P. Johanson-Blizzard syndrome. a new case with autopsy findings. *Genet. Couns.* **12**, 245–250 (2001).
14. Vieira, M.W. *et al.* [Johanson-Blizzard syndrome: the importance of differential diagnostic in pediatrics.]. *J. Pediatr. (Rio J.)* **78**, 433–436 (2002).
15. Zerres, K. & Holtgrave, E.A. The Johanson-Blizzard syndrome: report of a new case with special reference to the dentition and review of the literature. *Clin. Genet.* **30**, 177–183 (1986).
16. Cuschieri, A. Anorectal anomalies associated with or as part of other anomalies. *Am. J. Med. Genet.* **110**, 122–130 (2002).
17. Turner, G.C., Du, F. & Varshavsky, A. Peptides accelerate their uptake by activating a ubiquitin-dependent proteolytic pathway. *Nature* **405**, 579–583 (2000).
18. Pickart, C.M. Back to the future with ubiquitin. *Cell* **116**, 181–190 (2004).
19. Hershko, A., Ciechanover, A. & Varshavsky, A. The ubiquitin system. *Nat. Med.* **6**, 1073–1081 (2000).
20. Ciechanover, A. & Schwartz, A.L. The ubiquitin system: pathogenesis of human diseases and drug targeting. *Biochim. Biophys. Acta* **1695**, 3–17 (2004).
21. Jones, N.L., Hofley, P.M. & Durie, P.R. Pathophysiology of the pancreatic defect in Johanson-Blizzard syndrome: a disorder of acinar development. *J. Pediatr.* **125**, 406–408 (1994).
22. Halangk, W. *et al.* Trypsin activity is not involved in premature, intrapancreatic trypsinogen activation. *Am. J. Physiol. Gastrointest. Liver Physiol.* **282**, G367–G374 (2002).
23. Halangk, W. *et al.* Role of cathepsin B in intracellular trypsinogen activation and the onset of acute pancreatitis. *J. Clin. Invest.* **106**, 773–781 (2000).
24. Yin, J., Kwon, Y.T., Varshavsky, A. & Wang, W. RECQL4, mutated in the Rothmund-Thomson and RAPADILINO syndromes, interacts with ubiquitin ligases UBR1 and UBR2 of the N-end rule pathway. *Hum. Mol. Genet.* **13**, 2421–2430 (2004).
25. Kruger, B., Lerch, M.M. & Tessenow, W. Direct detection of premature protease activation in living pancreatic acinar cells. *Lab. Invest.* **78**, 763–764 (1998).
26. Mayerle, J. *et al.* Up-regulation, nuclear import, and tumor growth stimulation of the adhesion protein p120 in pancreatic cancer. *Gastroenterology* **124**, 949–960 (2003).
27. Kukor, Z. *et al.* Presence of cathepsin B in the human pancreatic secretory pathway and its role in trypsinogen activation during hereditary pancreatitis. *J. Biol. Chem.* **277**, 21389–21396 (2002).
28. Xie, Y. & Varshavsky, A. The E2–E3 interaction in the N-end rule pathway: the RING-H2 finger of E3 is required for the synthesis of multiubiquitin chain. *EMBO J.* **18**, 6832–6844 (1999).
29. Zeth, K. *et al.* Structural analysis of the adaptor protein ClpS in complex with the N-terminal domain of ClpA. *Nat. Struct. Biol.* **9**, 906–911 (2002).
30. Kwon, Y.T. *et al.* The mouse and human genes encoding the recognition component of the N-end rule pathway. *Proc. Natl. Acad. Sci. USA* **95**, 7898–7903 (1998).